SOLUTION MINING RESEARCH INSTITUTE

679 Plank Road
Clifton Park, NY 12065, USA

Telephone: +1 518-579-6587
www.solutionmining.org

Technical Conference Paper

1965 – 2025

Fast multicyclic storage of hydrogen in salt caverns

Matthias Brandt[1] Tobias Fabig[1]

[1] IfG - Institute for Geomechanics, Leipzig, Germany

Eddy Kuperus[2], Jeroen Dirven[2]

[2] Nederlandse Gasunie N.V, Groningen, The Netherlands

SMRI Spring 2025 Technical Conference
27-29 April 2025
Wilhelmshaven, Germany

Solution Mining Research Institute Spring 2025 Conference

Wilhelmshaven, Germany, 27-29 April 2025

Fast multicyclic storage of hydrogen in salt caverns

Matthias Brandt, Tobias Fabig

Institut für Gebirgsmechanik GmbH, Friederikenstraße 60, 04279 Leipzig, Germany

Eddy Kuperus, Jeroen Dirven

Nederlandse Gasunie N.V, Groningen, The Netherlands

Abstract

In general gas storage in rock salt caverns is a proven technology, and multicyclic use of gas storage caverns has been applied for over a decade. In addition to natural gas, the change of the energy system will likely result in the need to store hydrogen in underground caverns on a large scale. In recent years, the fraction of high frequency multi-cyclic operation mode has considerably increased, where more frequent loading and unloading cycles per year are applied. To establish the long-term conditions in which the caverns can be safely operated, a methodology has been developed based on rock-mechanical assessments on both cavern stability and the integrity of the barrier-forming salt rock mass. This methodology has been applied for over a decade in various gas storage projects.

The presented work is based on the above-mentioned methodology and includes over one decade of measured operational data for the cyclic storage of natural gas, and the same data is adapted to the storage of hydrogen in terms of the different thermodynamic properties. Additional worst-case considerations are carried out to confirm geo-mechanical stability and tightness under all possible usage cases.

The methodology provides:

- The proof of integrity shows that the tightness and stability of the rock salt around a hydrogen cavern is maintained even for the considered worst case scenarios.
- Moreover, the assessment proves that migration of gas along the casing of the borehole to the overburden can be excluded as the necessary horizontal confining stress is larger than the acting gas pressure inside the casing.
- Plastic deformations along the cavern contour are minimal. Under realistic operation conditions, cavern convergence remains limited, resulting only in limited subsidence.

Key words: gas storage, caverns for gas storage, cavern operation, rock mechanics, computer modeling

1. Introduction

In recent years the interest in underground hydrogen storage (UHS) in salt caverns has increased, due to the increasing necessity to store renewable energy. To ensure safe operation of these caverns in-situ tests were performed on boreholes and existing caverns. Some previous research work on the underground storage of hydrogen already exists. For example, experimental investigations were carried out in situ, to verify the ability of high-pressure storage of hydrogen in salt (HYPOS, 2022). Also,

the tightness of existing wellbores, the completion and the well head installation were carefully assessed and optimized in the A8 EnergyStock demonstration project.
To accompany these field studies, modelling of pressure-driven percolation was performed to demonstrate the stability and integrity of the storage caverns during the operating period (HYPOS, 2022). This general understanding of the potential processes occurring throughout the lifetime of an underground hydrogen storage cavern is applied while planning new cavern fields. Location specific properties of the salt mass have to be included, ideally according to the results of a lab program conducted on salt cores. Geomechanical effects of cyclic hydrogen storage in salt caverns are then examined based on scenario analyses. In the present work, we focus on the effects of rapid cycling. Basis for the assessment is definition of a theoretical maximum number of cycles per year, which is based on a pre-defined maximum pressure change per day, this maximum pressure change per day might be considered as conservative in itself and might be a topic for further assessment but is not part of this study. To evaluate the validity of the methodology real operational data has been used to test requirements and most critical points.
In the following geomechanical modelling, coupling of geomechanical processes to hydraulic and thermal processes is included. First, thermodynamical simulations of the pressure and temperature are carried out based on the planned cavern filling and gas production rates to obtain an approximate time dependence of temperature and pressure.
It is crucial to prove the stability and integrity of the planned caverns throughout their operational lifespan, often also including an abandonment period. Beyond that, one desired property of the operation of underground storage in salt at many sites is limited surface subsidence caused by cavern convergence.

The remainder of the paper is organized as follows:
In section 2 we describe the basics of the thermodynamic modelling yielding the pressure and temperature curves. In section 3 we summarize the methods of geomechanical modelling, how thermomechanical and hydraulic interaction are included, and how stability and integrity of the caverns are assessed. The results of the numerical modelling are presented in section 4. The paper concludes with a summary in section 5.

2. Basics of the thermodynamic modelling

In this work we have demonstrated the methodology carried out during the design phase of the caverns in the form of pressure and pressure change rate limits, verified by numerical simulations on one hand, and the results of a decade long operation of a natural gas storage site on the other. The chosen data set contains pressures, temperatures and especially the flow rates in normal cubic meters per day over a period of 10 years on an hourly basis.
Starting from the daily averaged flow rates and the initial temperature and pressure a prediction is made using a thermodynamic model developed at IfG. The pressure and temperature to be expected inside the cavern are recalculated for the case of hydrogen storage. The so calculated pressure and temperature are named the “field analogue data set” in the remainder of the paper. Then results of this procedure are given in Figure 2-1. As a comparison, a high frequency operation was simulated by the same thermodynamic model yielding the temperatures and pressure to be expected from fast multicyclic operation.
After having defined the cavern parameters the thermodynamic behavior is modelled in order to determine the temperature and pressure data that serve further cavern modeling. The cavern is simulated following field data for the storage operation in an existing natural gas storage cavern and high frequency hydrogen gas operation. In the high frequency modelling it is assumed that 10 t (22,000 lb) of hydrogen gas are produced from the cavern per hour as daily average from the cavern. The field data available was given in terms of norm cubic meters of natural gas per hour. The conversion to hydrogen was performed by keeping the volumetric gas flow rate the same. Production and storage rates peaked at about 12 t (26,500 lb) per hour but showed much smaller averages than for the assumed high frequency cycles.
In our methodology we introduce three pressure limits, the maximum pressure p_{max} (1), the minimum pressure p_{min} (2) and the minimum operational pressure $p_{min,o}$(3). For each pressure limit different quantities are relevant.
First, there is the maximum pressure p_{max} which is the pressure of the caverns that should never been exceeded for cavern integrity, set at the last cemented casing shoe depth. A common industrial guideline is to calculate the maximum gas pressure at the last cemented casing shoe that is admissible from

a gradient of $\gamma = 0.85 * \gamma_{overburden}$. As this is a mechanical condition, this limit does not differ, whether natural gas or hydrogen is considered.
Secondly, the minimum pressure p_{min} is derived from an empirical condition

$$(p_{MIN}) = 3.6MPa \cdot \left(\frac{H_{REF}}{1{,}000m}\right)^2,$$

and defines the pressure that the cavern can be at for a maximum of 30 days per year while ensuring that plastic deformation at the cavern contour remains limited.
And thirdly we introduce the pressure $p_{min,0}$ which is defined as the lower limit of the free operation range, between which the operator can choose to run the cavern at any pressure for any chosen time without substantial plastic damage to the cavern contour. The pressure in the cavern should not drop below $p_{min,0}$ for more than 90 days per year. The lower limit $(p_{MIN})_0$ of the free operation range is derived from the condition that the effective stress is only 90 % of the effective stress at minimum permissible storage pressure at give overburden pressure σ_G :

$$\sigma_G - (p_{MIN})_0 = 0.9 \cdot [\sigma_G - p_{MIN}]$$

All relevant pressures for our example of the operation of the gas storage are summarized in Table 2-1.

Table 2-1: Summary of the operational quantities in the cavern cycling as defined by empirical formulae

Operation quantity	Metric units	Imperial units
Maximum pressure p_{max}	180 bar	2610 psi
Minimum pressure p_{min}	55 bar	800 psi
Free operation pressure minimal $p_{min,0}$	80 bar	1160 psi

To quantify the temperature changes of the hydrogen stored within the cavern, thermodynamic simulations were carried out in a separate, thermodynamic model.
The nonstationary temperature field around the cavern and the heat exchange between the fluid in the cavern, the well and the surrounding rock are determined. The well is treated as cylindrical symmetric with equidistant pressure and temperature nodes, while the cavern is treated as a uniform spherical cavity with a single temperature and pressure. Heat transport from the cavern into the rock salt mass is calculated by a finite element method using this spherical symmetry.
The general numeric approach for the calculation of the temperature distribution in the well and cavern follows the equations given in the handbook for the SCTS 2.0 software (Nieland, 2004). The development of the tool was content of a SMRI research project. The temperature at the cavern wall is considered to be continuous, or in other words, a perfect thermal contact between the cavern and the rock salt is assumed.
The real gas thermodynamic properties of pure hydrogen are integrated with the help of the coolProp library 6.6.0 (Bell, Wronski, Quoilin, & Lemort, 2014). Vaporization of sump brine upon injection and condensation during the gas withdrawal phase are also considered. The vapor pressure of water is therefore calculated using Raoults law and the Buck equation, in an approach similar to that outlined in (Berest & Louvet, 2020)

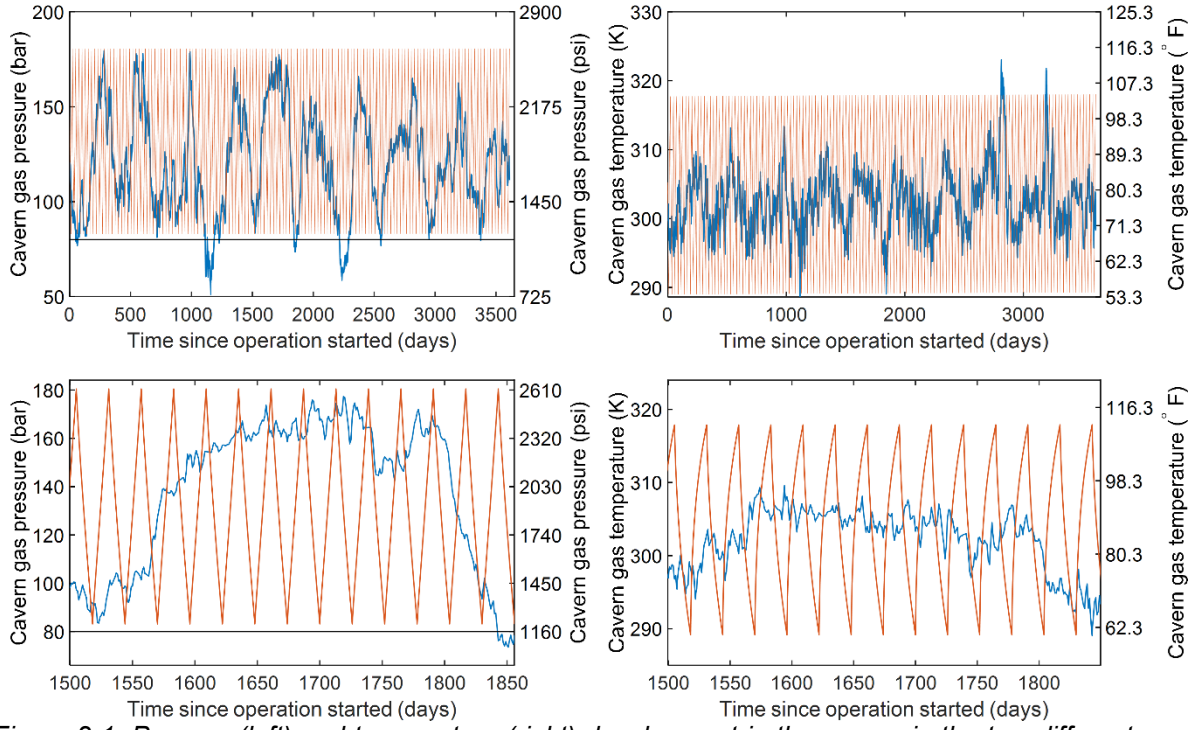

Figure 2-1: Pressure(left) and temperature (right) development in the cavern in the two different scenarios. The period between days 1,500 and 1,860 is magnified in the lower plot. The adapted pressures and temperatures from the field data are given in blue, the synthetic high frequency data is colored in red. The operational pressure limit $p_{min,o}$ is shown by a black line.

The expected cycling of the hydrogen storage cavern in the field analogue case is colored in blue in Figure 2-1. Especially from the pressure plot, the predominantly annual nature of the cycle can be seen. Ten distinct maxima and minima are visible. Likewise, ten maxima and minima are visible from the temperature plot; however, the field analogue data appears subject to more rapid changes than pressure. The temperature and pressure data however are both calculated from the same gas flow rates, and while the pressure is a nonlinear function of the total gas mass in the cavern, the temperature reacts more strongly to the current change in relative gas volume. However, please note that both pressure and temperature are function of each other, and of the whole history of the gas operations. Along with the field analogue data set, the synthetic data set is displayed, which consists of fourteen full cycles per year, with constant gas filling and extraction rates. Especially from the lower plots in Figure 2-1, which are limited to 360 days, it is visible, that the pressure in the cavern responds almost linearly to the constant gas filling or extraction rates, while the change in temperature is the highest at the beginning of the gas filling or extraction operation and then slowly decays.
It is also visible from the top plots that the field data analogue curves for the pressure fall below the pressure $p_{min,0}$ repeatedly for less than 90 days. The synthetic curves were chosen on purpose to remain above the limit of $p_{min,0}$, in order to simulate the free operation of the hydrogen cavern, and to ensure that the high filling and extraction rates simulated do not result in low cavern temperature and therefore tensile stresses at the cavern contour.
It is also visible that two peaks in temperature exist in the field analogue data which exceed the span of temperatures simulated in the synthetic high frequency cycles. These peaks must be attributed to the higher filling rates in the field analogue data, as compared to the synthetic high frequency data. This clearly shows the necessity that the filling and extraction rates in the synthetic data generation are well above the expected rates in the following field operation, at best above the technical achievable gas flow rates. For temperatures that are above the simulated range, no critical situation is expected, as these create more compressive stress in the cavern contour. However, if the temperature is below the modelled range, it is possible that additional tensile stresses at the cavern contour occur. In this case, local tensile failure of the contour zones cannot be excluded.

3. Description of geomechanical modelling

For the demonstration of the procedures employed during the modelling of a potential new hydrogen storage facility, we restrict ourselves to a model with a single cavern in limited dimensions in this paper.

Geometrically we limit our model to a single cavern inside an infinite rectangular grid of caverns with pillar width which are state of the art for the used cavern depth (Brückner, Schreiner, & Lindert, 2010) (Brückner, Minkley, & Lindert, 2011). The shape and depth of the cavern is based on the results of sonar measurements of a real-world example. The dimensions of the box-shaped model considered are 280 m (981 ft) in x, 320 m (1050 ft) in y and 2000 m (6562 ft) in z direction. The geometric layout with the location of the cavern is given in Figure 3-1.
The geology of the investigated model is simplified, with a thick uniform salt deposit and a single over-burden layer of 250 m (820 ft) thickness. Heterogeneity within the salt, and the possible proximity of the salt dome edge are not considered. The relevant information on the cavern is given in Table 3-1. The reference depth is defined to be at 1/3 of the cavern height above the sump.

Table 3-1: Summary of geometric quantities of the modelled cavern

Geometric quantity	Si value	Imperial value
Depth of casing shoe	1000 m	3280 ft
Depth of cavern roof	1060 m	3477 ft
Depth of cavern floor	1310 m	4298 ft
Reference depth	1230 m	4035 ft
Cavern volume	550,000 m^3	19.4 Mio. ft^3

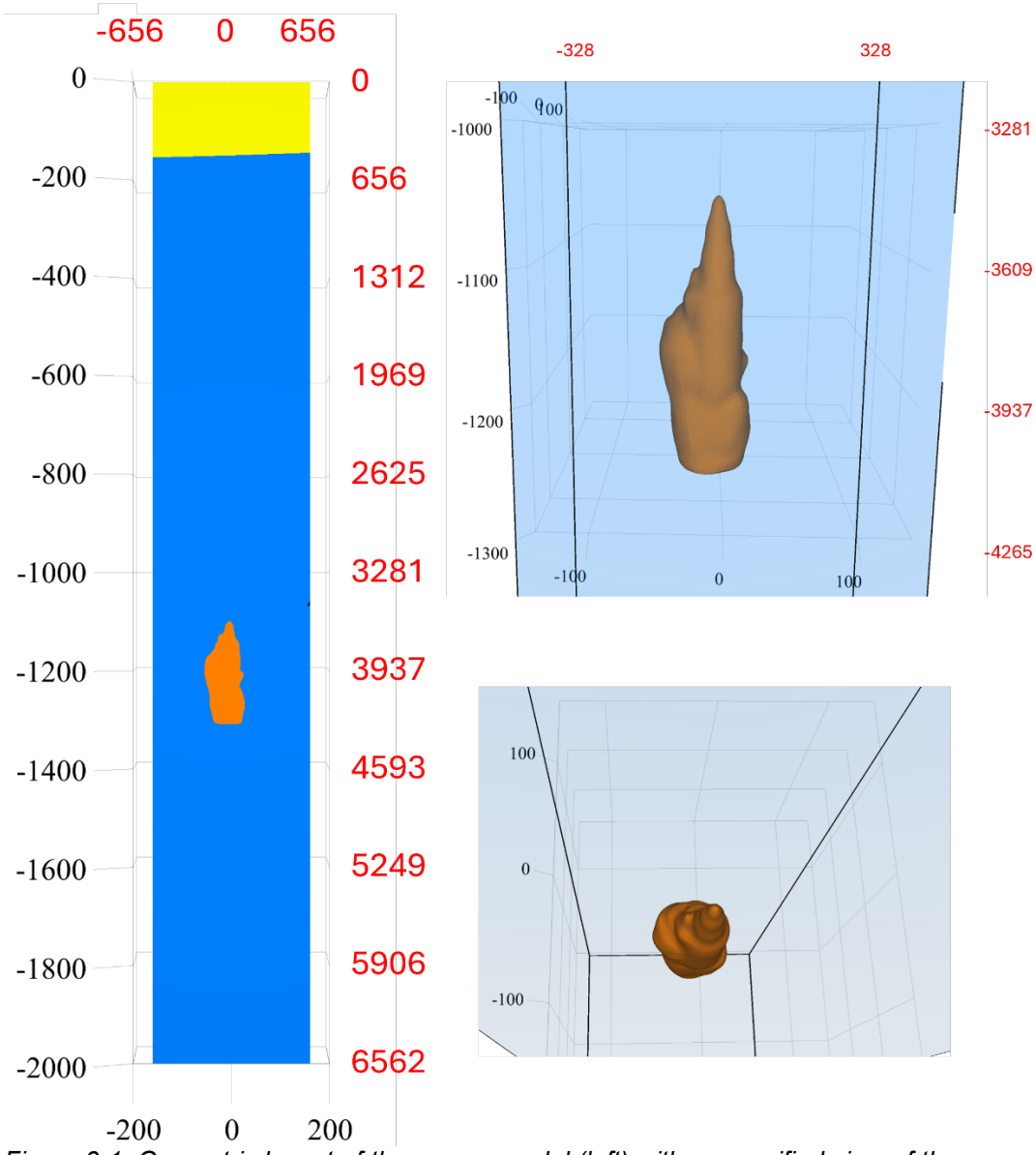

Figure 3-1: Geometric layout of the cavern model (left) with a magnified view of the cavern seen from the side (top right) and the top (bottom right), with the model box highlighted. All displayed dimensions in meters (black) and feet (red).

Within the modelling procedure the full history of the cavern is assessed, including leaching, a standstill phase, initial gas fill, and an operational phase. All computations are carried out using the Itasca software package FLAC3D, a continuum-mechanical finite-difference solver.
Both pressure and temperature curves as a function of time are applied to the cavern contour after the initial gas filling as a time-dependent boundary condition. During the gas storage operation mode within the model the stability and integrity were evaluated at multiple characteristic time-points by using criteria which are standard for the assessment of natural gas caverns (Brückner, Schreiner, & Lindert, 2010) (Brückner, Minkley, & Lindert, 2011).
The mechanical behavior of rock salt can be described within FLAC3D very accurately using customer-developed constitutive models. In the presented model, the Günther-Salzer model developed by the IfG (IfG-GS) was used. The behavior of rock salt can be modelled with high accuracy, and processes like damage generation and healing can be described. A good representation of all relevant creep processes is included, as well as a treatment of strain hardening and softening. A detailed description of the model and its capabilities is given in (Günther, Salzer, & Popp, 2010).
The overall creep rate is given as a function of von Mises stress σ_{eff} and the hardening variable ϵ_{cr}^{V}, that is implicitly defined as

$$\dot{\epsilon}_{cr}^{V} = A^{(p)} \exp\left(-\frac{\mathrm{Q_p}}{\mathrm{RT}}\right) \frac{\sigma_{eff}^{\beta}}{(\epsilon_0^V + \epsilon_{cr}^V)^{\mu}} - \dot{\epsilon}_{cr}^{E}$$

Here $A^{(p)}$, β and μ are material parameters and ϵ_0^V is the initial hardening.

Hardening is counteracted by dislocation annihilation, i.e., recovery. The recovery rate becomes higher for higher dislocation density and, since this is a thermally activated process, for higher temperatures. We assume a two- component power law for the recovery creep rate,

$$\dot{\epsilon}_{cr}^{E} = A_1^{(s)} \exp\left\{-\frac{Q_1}{RT}\right\} \sigma_{eff}^{n_1} + A_2^{(s)} \exp\left\{-\frac{Q_2}{RT}\right\} \sigma_{eff}^{n_2},$$

where $A_{1,2}^{(s)}$, $n_{1,2}$ and $Q_{1,2}$ are material parameters. We allow for two creep mechanisms with different activation energies Q_1 andQ_2, for a more precise adaptation of the temperature dependence.
The dilatant deformation of the rock salt dissipates energy. The work done on a unit volume is defined as,

$$U_{dil} = \int \langle \sigma_{eff} - \sigma_{eff}^{Dil} \rangle \, d\varepsilon_{cr}$$

On detailed procedures of how the actual dilatancy is computed, please refer e.g. to (Günther, Salzer, & Popp, 2010). The relevant parameters for the creep calculations are given in Table 3-2.

Table 3-2: Material parameters for rock salt

Rock Salt (Günther-Salzer Model)				
Parameter group	Quantity	Symbol	SI value	Imperial value
Elastic parameters	Density	ϱ	2180 kg/m^3	4.23 slug/ft^3
	Bulk modulus	K	20.7 GPa	3.0*10^6 psi
	Shear modulus	G	12.4 GPa	1.8*10^6 psi
Creep parameters	Transient creep			
	Prefactor	$A^{(p)}$	2*10^{-39} 1/d	2*10^{-39} 1/d
	Activation energy	Q_p	98 kJ/mol	93 BTU/mol
	Stress exponent	β	28.0	28.0
	Deformation exponent	μ	8.0	8.0
	Stationary creep term 1			
	Activation energy	Q_1	20 kJ/mol	19 BTU/mol
	Prefactor	A_1	7*10^{-4} MPa^{-1}d^{-1}	4.8*10^{-6} psi^{-1}d^{-1}
	Exponent	n_1	1	1
	Stationary creep term 2			
	Activation energy	Q_2	54 kJ/mol	51 BTU/mol
	Prefactor	A_2	0.035 MPa^{-5}d^{-1}	5.8*10^{-12} psi^{-5}d^{-1}
	Exponent	n_2	5	1

The FLAC3D software package is also able to perform coupled thermo-mechanical simulations. The initial thermal gradient in the salt dome and the surrounding rock salt is initiated and allowed to reach equilibrium under the given boundary conditions. Starting with the leaching process of the caverns, additional temperature boundary conditions are imposed on the cavern contour. The temperatures of the hydrogen during the storage phase are derived from the independent thermo-dynamic calculations as lined out in the previous section.
The thermal parameters applied to the model are listed in Table 3-3. For simplicity, no differentiation is made in the thermal conductivities and heat capacity of the salt and the overburden/surrounding rock. The temperature gradient is chosen that the situation in the salt dome can be reproduced correctly, ignoring the effects on the overburden. This results in an overestimation of the temperature at the ground surface, and an underestimation of the temperature gradient in the non-salt stratigraphic layers. The temperature gradient at the cavern location is not influenced by this.

Table 3-3: Parameters used for thermal modelling in FLAC3D

Thermal property	Symbol	SI value	Imperial value
Specific heat capacity	c_p	920 J/kg/K	0.22 BTU/(lb·°F)

Thermal conductivity	k	5,22 W/m/K	3.02 BTU/(hr·ft·°F)
Heat expansion coefficient	α	4*10^{-5} 1/K	7.2*10^{-5} 1/°F
Rock temperature	T	291 K – 0.022 K/m*z	63.8°F - 0.012°F/ft

3.1. Evaluation criteria

For the creation as well as long-term safe operation of caverns, the following rock-mechanical safety aspects are of essential importance (Minkley et al., 2005):

- Ensuring the stability of the caverns in the long-term. This includes ensuring:
  - the load-bearing capacity of the rock salt strata vaulting the caverns, considering the effective load of the overburden,
  - the stability of the pillars between neighboring caverns by considering the prevailing load exerted by the rock massif.

  The stability assessment requires that a sufficiently thick zone is found in the roof of the cavern or throughout the pillars, where the dilatancy criterion is not violated.
- Ensuring the geological tightness of the caverns, i.e. the rock salt zone which surrounds the cavern in a sufficient thickness prevents any contact of brine or any other fluid from the cavern with the biosphere or the overlying aquifers. Under undisturbed conditions, saliferous rocks are liquid- and even gas-tight. The pore volume of rock salt consists mainly of inter-crystalline cavities. A loss of tightness can be caused by the creation of connectivity, i.e., creation of interconnected crack-openings in the inter-crystalline structures. Tightness is ensured if the following two criteria are fulfilled: the minimum stress criterion (section 3.1.1) and the dilatancy criterion (section 3.1.2).

3.1.1. Minimum stress criterion for integrity

This criterion requires that inside a protective salt barrier the minor principal stress in the rock mass, σ_{min}, must always be higher than the internal pressure p_i in the cavern, to prevent fluid migration into the salt barrier. The criterion $\sigma_{min} > p_i$ can be expressed by defining a safety factor:

$$s_{fl} = \frac{\sigma_{min}}{p_i}$$

The minimum stress criterion is fulfilled if $s_{fl} > 1$, meaning that the permeation of fluid through the salt barrier is impossible. Due to the possibility of geological and operational uncertainties as well as additional thermodynamic effects that are not accounted for, such as even higher temporary flow rates than assumed in the preceding thermodynamic calculations, an additional 10% safety factor is included in the practical layout of a new gas storage cavern. The enhanced minimum principal stress criterion then becomes:

$$s_{fl} = \frac{\sigma_{min}}{p_i} > 1.1$$

3.1.2. Dilatancy criterion

This criterion requires that within the salt barrier no mechanical damage occurs, which would generate significant permeability (Peach C.J., 1996) (Popp T., 2001). The formation of (micro)cracks in the crystal structure is associated with an increase in volume, i.e., dilatancy. The load bearing capacity of these regions is significantly reduced, and permeability increases due to the connected network of oriented cracks. Thus, dilatant damage weakens the integrity of the barrier and therefore requires a respective assessment criterion. The dilatancy criterion is met as long as the volume $\varepsilon_{\mathrm{vol}}^{\mathrm{p}}$ is negative (elastic compaction) or maintained equal to zero (volume-retaining deformation):

$$\varepsilon_{\mathrm{vol}}^{\mathrm{p}} \leq 0$$

When the dilatancy boundary is exceeded, plastic volume dilatation will occur due to damaging processes: $\varepsilon_{\mathrm{vol}}^{\mathrm{p}} > 0$. Zones where plastic shear stains and dilatant deformation occur must be restricted to the rock mass zone directly behind the cavern. As long as the dilatancy stays below 1% in rock salt, damage accumulates, but the strain softening is not yet to be expected (Günther, Salzer, & Popp, 2010).

4. Results of geomechanical simulations

4.1. Simulation with field data analogue

First the results of the numerical simulations with the field data analogue pressures and temperatures will be discussed. For the illustration of the results, 5 different reference times are of relevance and will be referenced in the following. The first four points are situated before and after the steepest decline and incline in pressure in the cavern respectively, the fifth is simply the endpoint of the 10 years of operation.
The first reference point is located after 1195 days of hydrogen operation, the second after 1845 days. For illustrative purposes, the relevant region in the pressure and temperature curves is enlarged in Figure 2-1, bottom. All pressures and temperatures at all reference points are given in Table 4-1.
While the pressure decreases below the $p_{min,0}$ also the temperature is among the lowest calculated in the 10 years of operation modelled. Likewise, the third reference point is found after 2291 days, and the fourth after 2371 days. Between these days, one of the largest filling rates of 8 t/h was applied to the cavern, resulting in a sharp increase in temperature up to 44.9°C, which is the highest temperature simulated in the ten years of operation. These four points were chosen for their extreme conditions in the cavern and will now be investigated in detail.

Table 4-1: pressure and temperature conditions at the reference points

# of point	Time [d]	p [bar]	T [°C]	p [psi]	T [F]
1	1795	160	29.2	2320	84.6
2	1845	74	20.2	1073	68.4
3	2291	126	28.5	1827	83.3
4	2371	157	44.9	2277	112.8
5	3650	111	25.4	1609	77.7

The stress conditions found in the vicinity of the cavern are displayed in Figure 4-1. Both the major principle and minor principal stress are shown. The color bar of the plot is limited to 20 MPa, a value that is reached about 150 m above the roof of the cavern in the undisturbed rock conditions. Any color other than blue therefore indicates a significant reduction of stress as a consequence of the gas storage operation. For the major principal stress such a significant reduction is only visible at reference points 2 and 3, which are both occurring at low pressure and temperature. A reduction of the minor principal stress is visible for all the reference points, but is most pronounced at point two, where the pressure in the cavern is below $p_{min,0}$, and the temperature is about 290 K (compare Figure 2-1 and Figure 4-2). Compared to reference point 1, the minimum principal stress is about 12 MPa lower. Nonetheless, the minimum principal stress remains compressive, with a value of at least 3 MPa, indicating that even in the most extreme conditions during the cycle, tensile fractures are not to be expected. It is interesting to note that the minimum principal stress is the lowest in parts of the cavern with a cavern contour, i.e. where regions of the contour are protruding into the cavern.
The minimum principal stress at reference point 3 is lower than at reference point 1, but about 8 MPa above that at reference point 2. From that on, both the temperature and pressure in the cavern increase, resulting in a pronounced increase in the minimum principal stress towards reference point 4. The minimum principal stress is then higher than at reference point 1, especially in areas where there is a pronounced convex curvature, i.e. a contour element has more contact with the rock mass, than to the cavern void.

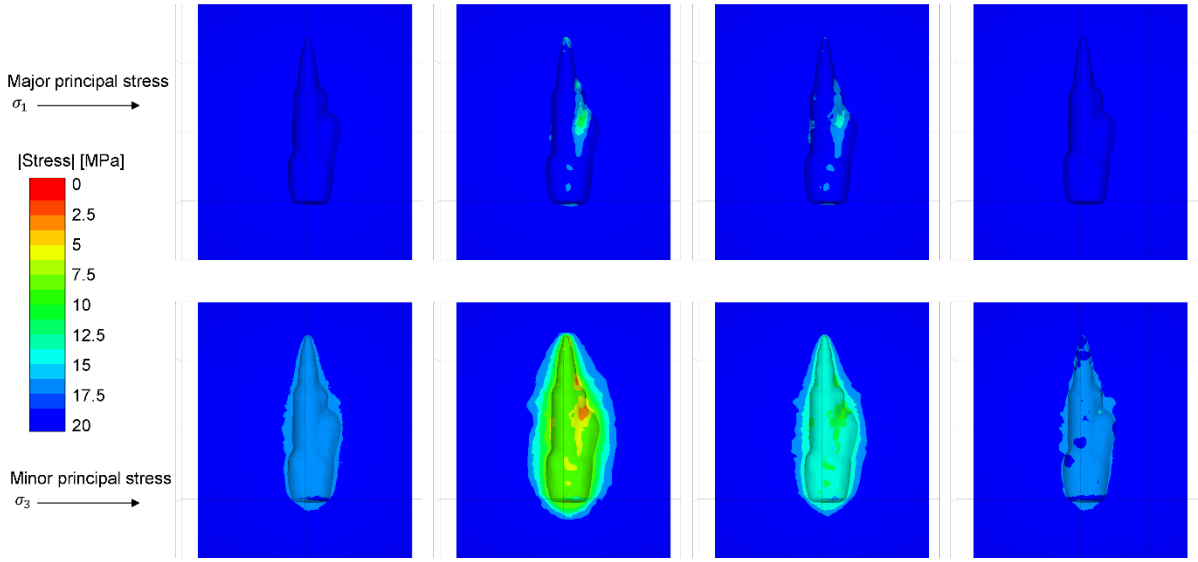

Figure 4-1: Major (most compressive, top) and minor (least compressive, bottom) stress in the cavern at reference point (from left to right) 1 (before a large pressure decrease), 2 (after a large pressure decrease, 3 (before a fast pressure increase), and 4 (after a fast pressure increase).

The temperatures during the cycles are given in Figure 4-2, top row. In the model a perfect thermal contact between the gas in the cavern and a single uniform temperature in the cavern is assumed. This is a conservative assumption, as in reality there is a finite resistance to heat transport at the contour, and the temperature will be closer to the initial temperature in the rock mass. The temperature in the cavern contour, as depicted in Figure 4-2, is therefore very close to the temperatures from the thermodynamic simulation that are given as a boundary condition at the cavern contour. The history of the cavern temperature however still influences the temperature behind the first cavern contour elements, as can be seen for example at reference point 4, were, in spite of a high temperature at the cavern contour of about 50 °C, the temperature a few meters from the cavern contour is about 35 °C and again increases along a trajectory normal to the cavern contour. The reason for the observed behavior is the finite heat conductivity of the salt. Therefore, the history of the temperature cycling has direct consequences on the stress field, and therefore on stability and integrity of the cavern.
The stability and integrity of the cavern are assessed by the help of the two criteria, as mentioned above in section 3.1.

First, we assess the minimum principal stress criterion. The results of the evaluation of this criterion are displayed in Figure 4-2, bottom row for the four reference points. Three colors are used in the graph, namely blue, which corresponds to a $s_{\mathrm{fl}} > 1.1$ meaning, that the minimum principal stress criterion is fulfilled including an additional 10% safety, green which corresponds to $1.1 > s_{\mathrm{fl}} > 1.0$ which means, that the minimum principal stress criterion is fulfilled without an additional safety and red which corresponds to $s_{fl} < 1.0$ which means, that the minimum principal stress criterion is violated.
Two very general statements can be given at first glance, namely, that at all four refence points the minimum principal stress criterion is violated somewhere around the cavern contour and that this violation of the minimum principal stress criterion never extends very deep into the cavern contour, typically only for a few meters.

Consequently, a migration of hydrogen into the contour is expected, but the region to where it can migrate will be limited. At a more detailed look at the results, some regions always show a violation of the minimum principal stress criterion without additional safety, which are mostly regions where the contour locally shows a concave curvature, i.e. overhanging parts. These regions have a larger relative fraction of their surface exposed to the cavern and therefore are more subject to the temperature and pressure changes in the cavern. As the pressure in the cavern is always below that in the undisturbed rock, the minimum principal stress is reduced in these areas as discussed before, and therefore a violation of the minimum principal stress criterion is most likely in these areas. The affected volumes of rock salt will therefore be subject to a slow percolation of hydrogen into them, and in the operational reality of caverns it is known that such regions are most affected by flaking and rock fall events, which over time however reduced the overhang in these regions, resulting in a smoother contour.

Next, it is visible that certain parts of the cavern contour see changes in between the minimum principal stress criterion being violated and being fulfilled. The situation with respect to the minimum principal stress criterion without additional safety is worse when the pressure is low, see reference points 2 and 3. This is a consequence of the fact that at the same time as the pressure being low, also the temperature at the cavern contour is low, which results in an additional reduction of the minimum principal stress. This statement is intuitive, however the direction of the action of pressure and temperature is not identical, the pressure acts normal to the cavern surface, while the temperature results in an all-sided contraction of the rock salt, and therefore also contains a tangential component. As displayed in Figure 2-1, temperature and pressure do not follow the same tendency. The pressure follows the total gas content in the cavern, while temperature is more tied to its time derivative. Overall, pressure and temperature do also depend on the history of the gas operation. The following geomechanical calculation depends on the history of the gas handling as well and a precise description requires to be calculated in a coupled time dependent model, as the presented one in here.

Following a reduction of the pressure and temperature as seen between reference point 1 and 2, the regions in which the minimum principal stress criterion with an additional safety factor is violated decreases. The same is visible for the increase in temperature and pressure as seen between reference points 3 and 4, where both the regions where the minimum principal stress criterion with and without safety factor is violated, decrease. This is to be considered the effect of the rapidly increasing temperature. It has to be concluded that if the pressure remains within the allowed limits, an increase of the temperature beyond the modelled frame has no negative impact on the minimum principal stress criterion.

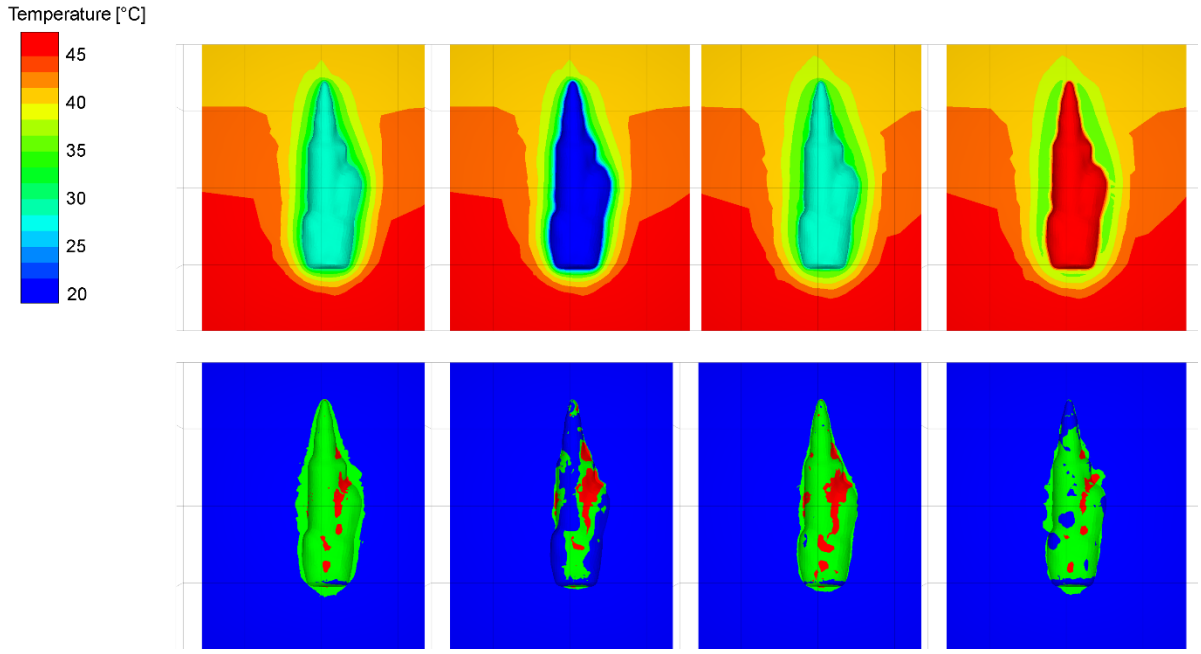

Figure 4-2: Temperature (top, according to color bar) and results of the evaluation of the minimum principal stress criterion (bottom, colors according to text) reference point (from left to right) 1 (before a large pressure decrease), 2 (after a large pressure decrease, 3 (before a fast pressure increase), and 4 (after a fast pressure increase).

Secondly, we assess the dilatancy criterion. The dilatant volume deformation is divided into parts created by shear and tensile deformation and is given in Figure 4-3. The dilatant deformation does not change visibly between the reference points, the component by shear deformation is always larger than the one by tensile deformation, and both are found roughly in the same location. Finally, the spatial extent of the dilatant deformation remains localized to the cavern contour, and small in magnitude. A threat to cavern stability by dilatant deformation is not to be expected as long as the cavern pressure remains above the stated minimal pressure. It is also visible that regions where the minimum principal stress criterion is continuously violated are also subject to dilatant damage.

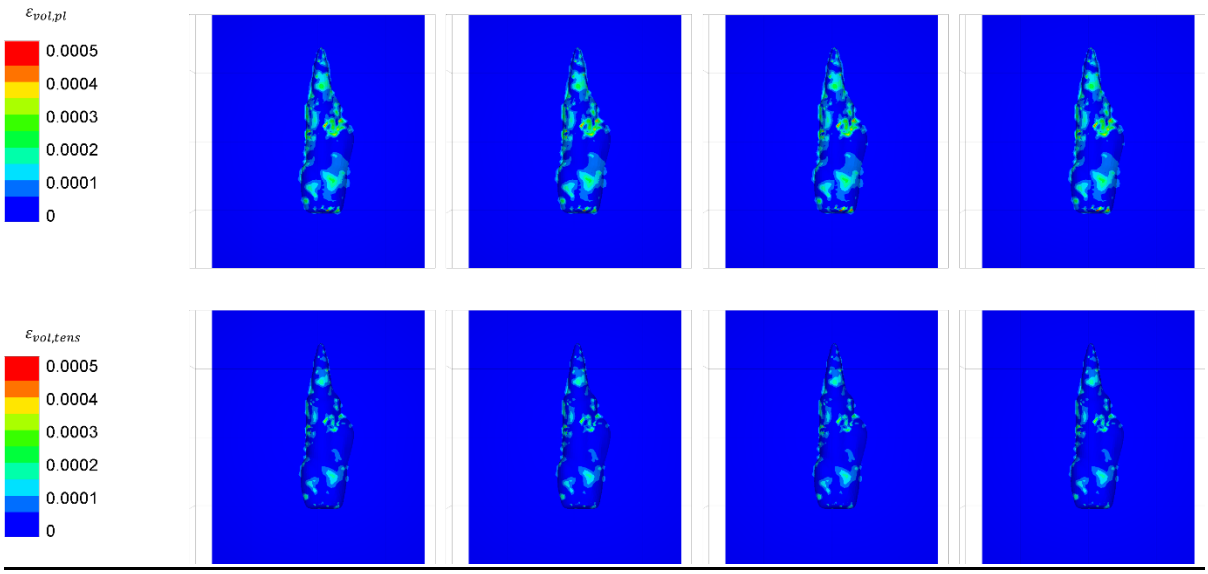

Figure 4-3 Dilatancy introduced by shear (top) and tensile (bottom) plastic deformation for the four reference points

4.2. Simulation with high frequency synthetic data

In addition to the simulations with the field analogue data, we carried out another simulation with the synthetic data set, as depicted in Figure 2-1, red curve.

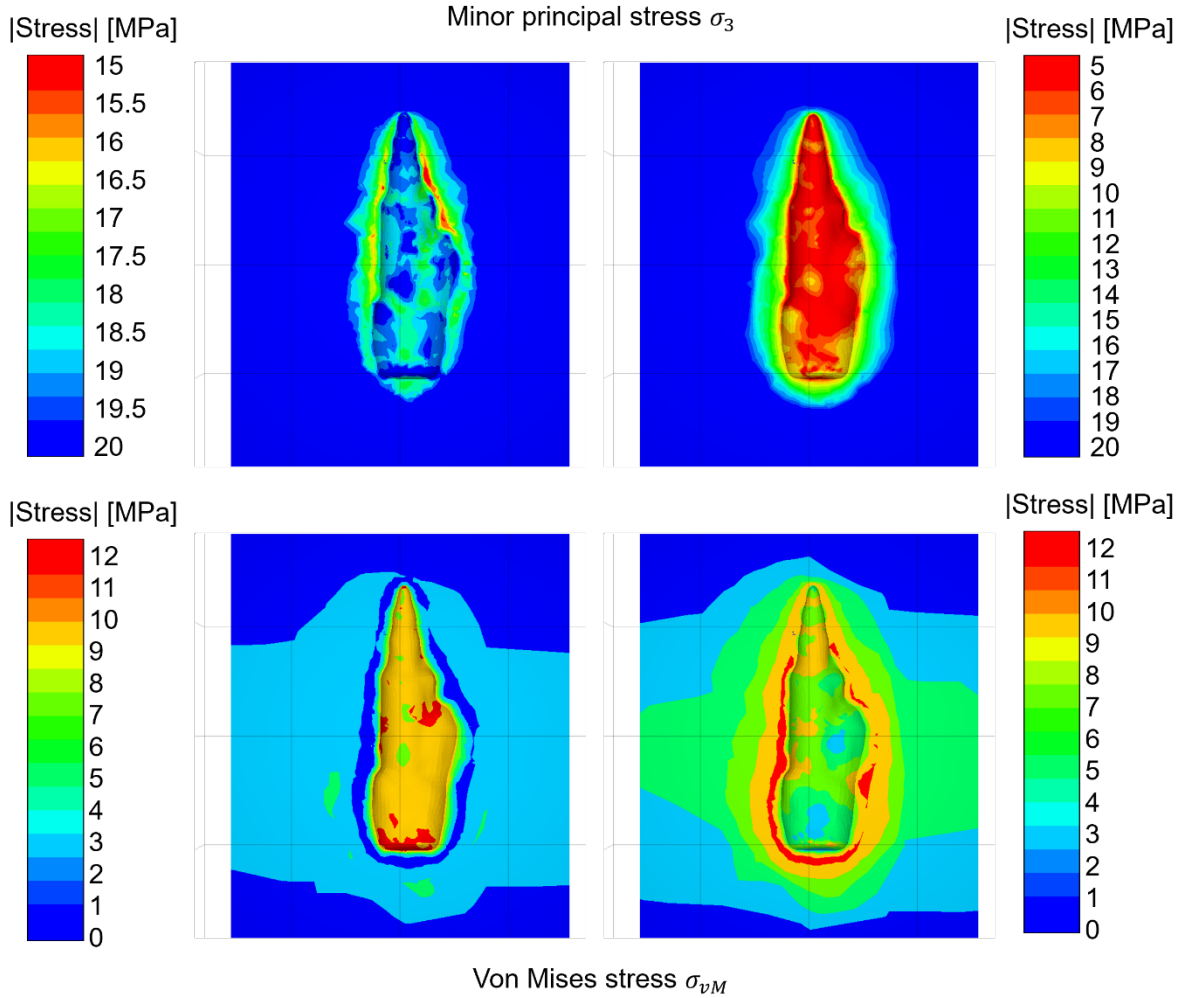

Figure 4-4: Minor principal stress (top) and von-Mises stress at the maximum (left) and minimum pressure (right) during the high frequency synthetic cycles. Note the different scales in each subplot

The results for the stress state are shown in Figure 4-4. The minimum principal stress is given at the top, and the von Mises equivalent stress at the bottom. The situation at the maximum pressure is shown on the left, that at the minimum pressure on the right. What can be noticed is that beyond the change in magnitude, also the localization of the minimum principal stress changes. While for the minimum pressure, the minimum of the minimum principal stress is clearly located at the cavern contour, it is found in a small distance from the cavern contour at the maximum pressure. This is explained by the fact, that also the temperature has reached a maximum when the pressure is at maximum, but (as can be seen from Figure 4-5, top), the speed at which the temperature change propagates into the rock mass is limited by its thermal conductivity, while that of the stress change is limited by the speed of sound. The thermal expansion of the rock salt is therefore high at the cavern contour, resulting in a thin layer, where the stress is more compressive than behind the contour, where the stress is still lower. This thin layer also leads to a more favorable situation, when regarding the minimum principal stress criterion. The region where a violation of the minimum principal stress is most pronounced is not always directly at the cavern contour, but a few meters behind it, where temperatures and therefore minimum principal stress remains lowered. In total the region where the minimum principal stress criterion is violated is much larger at maximum pressure, than at minimum pressure, and also than anywhere during the field data analogue cycles modelled. This is a consequence of the high extraction rates, and the fact that these gas extractions are uninterrupted from the minimum to the maximum. It is important to note that, in the assessment of the zone where the minimum principal stress criterion is violated, the maximum extent throughout a cycle must be considered. Under these conditions, the high frequency cycles clearly provide a conservative envelope for the field data analogue cycles regarding the extent of the violation of the minimum principal stress criterion.

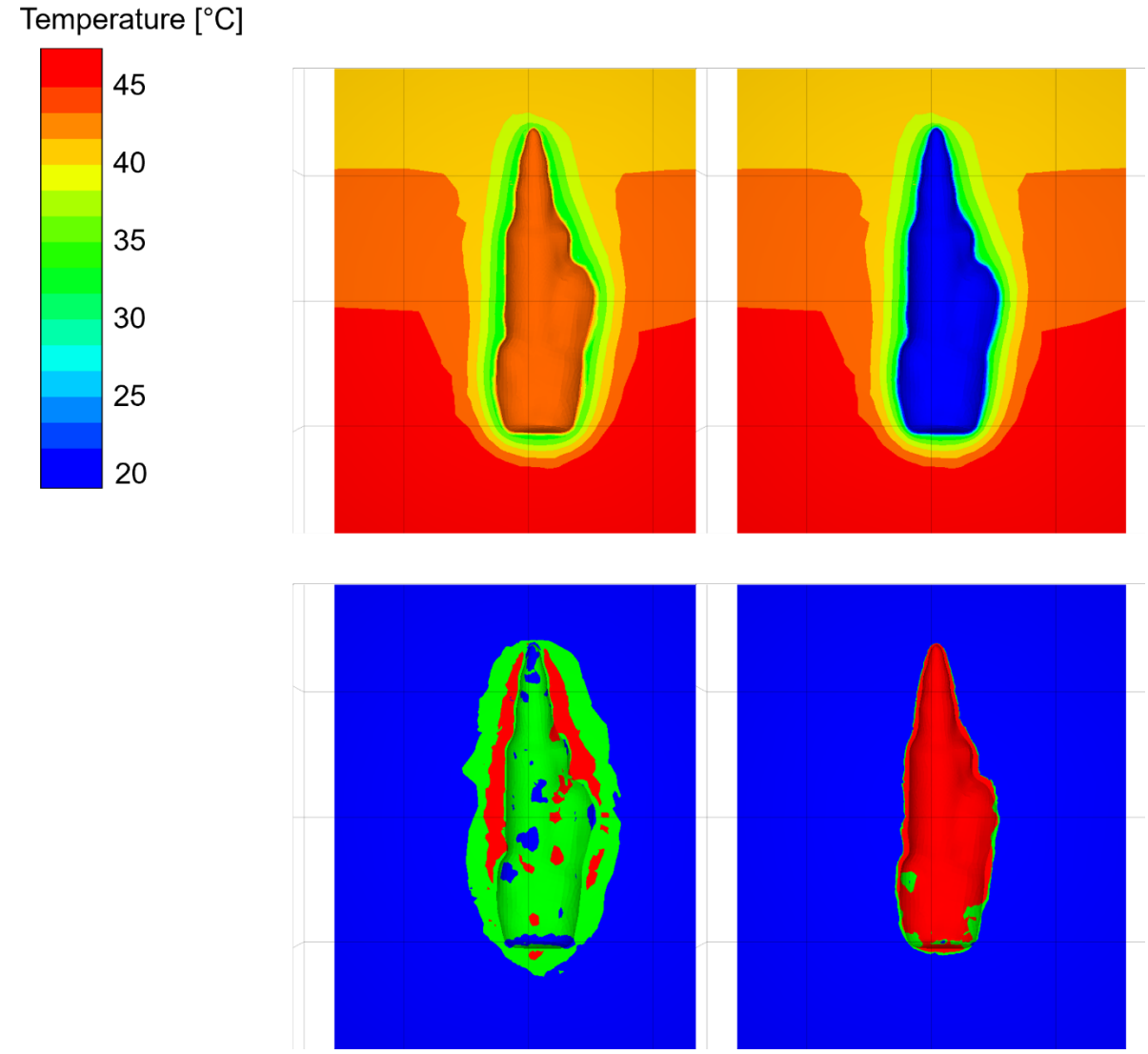

Figure 4-5: Temperature (top, according to color bar) and results of the evaluation of the minimum principal stress criterion (bottom, colors according to text) at a maximum (left) and minimum pressure (right) during the high frequency synthetic cycles.

Nonetheless, the minimum principal stress is not violated in most of the pillars, when this maximum extent of the violation of the minimum principal stress is considered. The region where dilatant damage of the cavern contour appears in general is much smaller in extent, than the region where the minimum principal stress criterion is violated.

5. Conclusion

In this document we presented a methodology to assess the stability and integrity of a salt cavern used for multi-cyclic storage operation mode. By means of this methodology safe operational boundary conditions are defined. This methodology has been applied in salt caverns used for decades of gas storage, and measured multi cyclic operational cavern data has been used to confirm assessment.

This methodology provides a means to assess the possible use for multicyclic operation of a hydrogen storage cavern use. It can be stated that:

- The minimum principal stress criterion is fulfilled in the pillar and overburden except for a few meters around the cavern, in which it is violated.
- The precise regions in which it is violated do vary according to pressure and temperature conditions.
- High temperatures more than the ones used during the layout simulation of the cavern do not produce an additional risk if pressures do remain in the intended range.
- Low temperatures can produce risks and must therefore be carefully excluded by the limitation of gas flow or pressure change rates. This is guaranteed by the proven concept of different pressure limits. The lower limit of the free operational range $p_{min,o}$ is the limit, below which the pressure in the cavern can only be changed by a reduced pressure change rate for less than 90 d/yr. The total lower limit for the cavern internal pressure p_{min} which is associated with a time limit of 30 d/yr that the pressure can stand at this point.
- Even with the change of the region violating the minimum principal stress criterion most of the pillar and the cavern roof are never affected by a violation of the minimum principal stress criterion or the dilatancy criterion. Stability and integrity of the cavern are therefore guaranteed under both the field analogue cycling and the synthetic high frequency cycling.
- Even with this conservative assumption, the area in which the minimum principal stress criterion was violated remains limited, and it can be concluded that the underlying design principles used when deciding the allowed range of the operational cycle were sufficiently conservative to allow for safe operation throughout the long-term operation mode.

References

Bell, I., Wronski, J., Quoilin, S., & Lemort, V. (2014). Pure and Pseudo-pure Fluid Thermophysical Property Evaluation and the Open-Source Thermophysical Property Library CoolProp. *Industrial & Engineering Chemistry Research*, pp. 2498 - 2508.

Bérest, P., & Louvet, F. (2020). Aspects of the thermodynamic behavior of salt caverns used for gas storage. *Oil & Gas Science and Technology – Rev. IFP Energies nouvelles, 75*(57).

Brückner, D., Minkley, W., & Lindert, A. (2011). The improved IfG Gas Storage Cavern Design Concept. York: SMRI Fall 2011 Technical Conference.

Brückner, D., Schreiner, W., & Lindert, A. (2010). IfG Cavern Design Concept Rockmechanical aspects for the development and operation of rock salt caverns. Leipzig: SMRI Fall 2010 Technical Conference.

Günther, R.-M., Salzer, K., & Popp, T. (2010). Avanced strain - hardening approach constitutive mpdel for rock salt describing transient, stationary, and accelerated creep and dilatancy. 44th U.S. Rock Mechanics Symposium and 5th U.S.-Canada Rock Mechanics Symposium: ARMA–10–495.

HYPOS. (2022). *Leitfaden Planung, Genehmigung und Betrieb von Wasserstoff-Kavernenspeichern.* Leipzig.

Nieland, J. D. (2004). *SALT CAVERN THERMAL SIMULATOR USER'S MANUAL* (2.0 ed.). Rapid City: Respec.